HHS Public Access

Author manuscript

J Am Chem Soc. Author manuscript; available in PMC 2021 March 31.

Published in final edited form as:

J Am Chem Soc. 2018 October 03; 140(39): 12424–12433. doi:10.1021/jacs.8b05147.

Cell-Permeable Activity-Based Ubiquitin Probes Enable Intracellular Profiling of Human Deubiquitinases

Weijun Gui[†], **Christine A. Ott**[†], **Kun Yang**, **Jedidiah S. Chung**, **Siqi Shen**, **Zhihao Zhuang**[*]

Department of Chemistry and Biochemistry, University of Delaware, 214A Drake Hall, Newark, Delaware 19716, United States

Abstract

Advancement in our knowledge of deubiquitinases (DUBs) and their biological functions requires biochemical tools permitting interrogation of DUB activities under physiologically relevant conditions. Activity-based DUB probes (DUB ABPs) have been widely used in investigating the function and activity of DUBs. However, most ubiquitin (Ub)-based DUB ABPs are not cell-permeable, limiting their utility to purified proteins and cell lysates. Lysis of cells usually leads to dilution of the cytoplasm and disruption of the normal cellular organization, which may alter the activity of many DUBs and DUB complexes. Here, we report a new class of cell-permeable DUB ABPs that enable intracellular DUB profiling. We used a semisynthetic approach to generate modular ubiquitin-based DUB probes containing a reactive warhead for covalent trapping of DUBs with a catalytic cysteine. We employed cell-penetrating peptides (CPPs), particualrly cyclic polyarginine (cR_{10}), to deliver the DUB ABPs into cells, as confirmed using live-cell fluorescence microscopy and DUB ABPs containing a fluorophore at the C-terminus of Ub. In comparison to TAT, enhanced intacellular delivery was observed through conjugation of a cyclic polyarginine (cR_{10}) to the N-terminus of ubiquitin via a disulfide linkage. Using the new cell-permeable DUB ABPs, we carried out DUB profiling in intact HeLa cells, and identified active DUBs using immunocapture and label-free quantitative mass spectrometry. Additionally, we demonstrated that the cell-permeable DUB ABPs can be used in assessing the inhibition of DUBs by small-molecule inhibitors in intact cells. Our results indicate that cell-permeable DUB ABPs hold great promise in providing a better understanding of the cellular functions of DUBs and advancing drug discovery efforts targeting human DUBs.

Graphical Abstract

[*]Corresponding Author: zzhuang@udel.edu.

[†]Author Contributions

W.G. and C.A.O. contributed equally to this work.

Supporting Information

The Supporting Information is available free of charge on the ACS Publications website at DOI: 10.1021/jacs.8b05147.

Figures, tables, and methods; synthetic schemes; and characterization of new compounds (PDF)

The authors declare no competing financial interest.

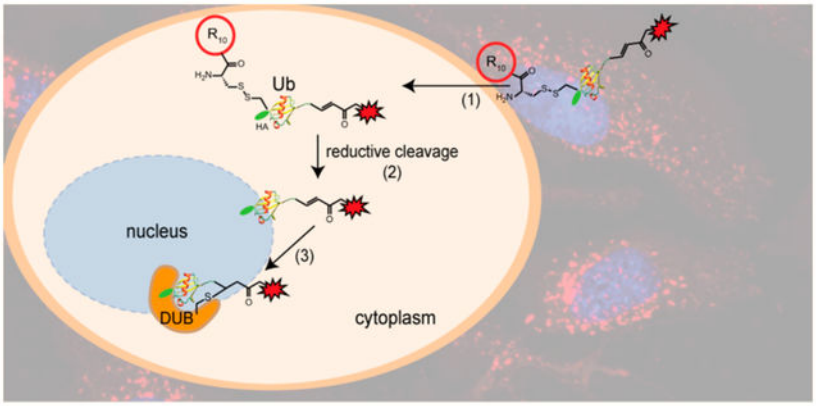

INTRODUCTION

Ubiquitination is an important, reversible post-translational modification (PTM) in eukaryotic cells. Ubiquitination is catalyzed by a three-enzyme cascade (E1–E2–E3) culminating in the attachment of the C-terminal carboxylate of ubiquitin (Ub) to an ε-amino group of a lysine residue in the acceptor protein via an isopeptide bond.[1] Deubiquitinating enzymes (DUBs) oppose this process by removing mono-Ub and poly-Ub chains from substrate proteins in various cellular pathways. In recent years, DUBs have emerged as promising targets for drug development, notably in cancer and neuro-degeneration.[2] Activity-based DUB probes (ABPs) have facilitated the development of DUB inhibitors and allowed profiling of DUB activities in cell lysates.[2–16] A full understanding of the cellular function of DUBs is crucial for the development of next generation therapeutics to treat a range of human diseases.

The most widely employed DUB activity-based probes contain a mono-Ub recognition element with an electrophilic group conjugated to its C-terminus, exemplified by Ub propargylamide (Ub-PA) or Ub vinyl methyl ester (Ub-VME).[17–21] Recently, the Ub-based DUB probes have expanded to include internal and terminal diUb-based ABPs,[22–26] ubiquitin photoaffinity probes,[27,28] ubiquitin interactor affinity probes,[29,30] Ub-substrate probes,[31,32] and a reactive-site-centric DUB probe.[33] The above-mentioned DUB ABPs have greatly enhanced our knowledge of DUBs through elucidation of linkage specificity,[22–26] structural determination of DUB-Ub cocrystal structures,[34–39] and the development of DUB inhibitors.

Currently, most Ub-based DUB ABPs are cell-impermeable, thus limiting their utility to purified proteins and cell lysates. Cell lysate-based DUB profiling has been widely used and considered to better reflect the native function and regulation of DUBs. However, lysing cells usually causes a dilution of the cytoplasmic and nuclear proteins, leading to potential dissociation of protein complexes necessary for DUB activity. The disruption of cellular organization may also affect the DUBs' activity and regulation. Therefore, there is a need for DUB ABPs that can penetrate the cell plasma membrane and capture DUBs within intact cells. This class of DUB ABPs will further expand our knowledge of the biological functions of DUBs in a physiologically relevant setting. Several efforts have already been

made in this area, including catch-and-release probes and the use of a pore-forming toxin perfringolysin O (PFO) to facilitate entry of Ub-based ABPs into semi-intact cells.[40] A small-molecule DUB ABP was reported, with which 12 ubiquitin-specific proteases (USP) were identified using mass spectrometry (MS)-based quantitative proteomics.[41] In another report, electroporation was used to deliver the ubiquitin cascade activity-based probe (Ub-Dha) into human cells.[42] In addition to the labeling of enzymes in ubiquitin cascade (2 E1's, 19 E2's, 2 E2/E3's, and 2 E3's), four DUBs were labeled and identified using MS-based quantitative proteomics.

In this study, we report the generation of a new class of cell-permeable DUB ABPs, which can efficiently enter intact HeLa cells and enable intracellular DUB profiling. Chemoselective conjugation strategies were utilized to attach a thiol-reactive warhead to the ubiquitin C-terminus and a polycationic cell-penetrating peptide (CPP), particularly a cyclic polyarginine peptide (cR_{10}), to the N-terminus of the Ub-based DUB ABPs to achieve cell membrane penetration. Efficient uptake of the newly developed cell-permeable DUB ABPs was confirmed using live-cell fluorescence confocal microscopy. Cell-permeable DUB ABPs allowed us to carry out intracellular DUB profiling analyzed by immunoblotting and MS-based quantitative proteomics analysis. A pan-DUB inhibitor, PR-619, was used as a proof of concept to demonstrate the utility of our cell-permeable DUB ABPs in DUB inhibitor discovery. Our approach of activity-based DUB profiling, using cell-permeable DUB ABPs, minimizes the disruption to the cellular and subcellular organization of cells, and therefore holds great potential for providing physiologically relevant insights into the biological function and activity of human DUBs.

RESULTS AND DISCUSSION

Generation of Cell-Permeable Ub-Based DUB ABPs.

Ubiquitin, being a small protein, cannot penetrate the plasma membrane of human cells. To circumvent this, our strategy employs cell-penetrating peptides (CPPs) to facilitate the uptake of Ub-based probes by human cells. CPPs have been reported as versatile delivery vehicles for cell-impermeable molecules, including oligonucleotides, proteins, peptides, siRNAs, and nanoparticles.[43] In this study, we designed a new class of cell-permeable Ub-based DUB ABPs for intracellular DUB profiling.

Our initial efforts utilized TAT (a.a. KRKKRRQRRR) peptide, through expression as a linear fusion to the N-terminus of HA-$Ub_{1–75}$ to generate a cell-permeable Ub-based DUB ABP. To generate the probe, TAT-HA-$Ub_{1–75}$ was expressed and purified as an intein fusion and cleaved with sodium 2-mercaptoethanesulfonate (MESNA). TAT-HA-$Ub_{1–75}$-MESNA was then reacted with propargylamine (PA) generating TAT-HA-Ub-PA (**1**) (Scheme S1).

Recently, cyclic polyarginine (cR_{10}) peptide was found to enhance the cellular uptake of protein cargos as compared to both linear and cyclic TAT peptides.[44–46] The enhancement was attributed to increased membrane contacts due to the increased number of arginine residues and the more rigid cyclic backbone structure.[44,47] The cellular entry of cargos via arginine-rich CPPs, including TAT and cR_{10}, is thought to be through an energy-independent direct penetration of the cellular membrane.[44–47] We devised an Ub-based DUB ABP

containing a disulfide-linked cR_{10} peptide at the N-terminus of the probe as shown in Figure 1a. Solid-phase peptide synthesis was used to generate cR_{10} as previously reported with minor modifications (Scheme S2).[46] We then generated HA-Cys-(cR_{10})-Ub-PA, in which cR_{10} is linked to HA-Cys-Ub-PA through a disulfide bond (Figure 1a). The disulfide bond is known to be cleaved upon entry into cells with a reducing environment.[48] This generates HA-Cys-Ub-PA, a close mimic of the commonly utilized DUB ABP, HA-Ub-PA. To generate the above-described cell-permeable DUB ABP, site-directed mutagenesis was first used to introduce a cysteine residue between the HA-tag and the N-terminus of $Ub_{1–75}$, which we named HA-Cys-Ub. Using an intein-based purification method similar to TAT-HA-Ub-MESNA, HA-Cys-Ub-MESNA was purified. The cysteine residue was then protected using 5,5′-dithiobis(2-nitrobenzoic acid) (DTNB) to generate HA-Cys(TNB)-Ub-MESNA. Propargylamine was then reacted with HA-Cys(TNB)-Ub-MESNA to generate HA-Cys-(TNB)-Ub-PA. HA-Cys(TNB)-Ub-PA was subsequently reacted with cR_{10}, through disulfide bond exchange reaction, to yield HA-Cys(cR_{10})-Ub-PA (**2**). Following HPLC purification, lyophilization, and refolding in MES buffer (50 mM MES, 100 mM NaCl, pH 6.5), the identity of probe **2** was confirmed by ESI–MS analysis. The observed mass of 11 939 Da is identical to the calculated molecular weight of 11 939 Da (Figure 1b).

Next, we sought to generate two other cR_{10}-containing cell-permeable probes, HA-Cys(cR_{10})-Ub-VME (**3**) and HA-Cys(cR_{10})-Ub-EA (**4**), using a similar method. The structure of probe **3** and **4** is shown in Figure 1c. HA-Cys(cR_{10})-Ub-VME (**3**) contains another widely used cysteine-reactive warhead vinyl methyl ester (VME) for DUB profiling (Scheme S3). Moreover, we generated a control probe that is cell-permeable, but contains an unreactive ethylamine at C-terminus, HA-Cys(cR_{10})-Ub-EA (**4**) (Scheme S4).

In Vitro Labeling of DUBs Using Cell-Permeable Ub-Based DUB ABPs.

With the cell-permeable DUB ABPs in hand, we assessed their reactivity using recombinantly purified USP2 catalytic domain (USP2-CD). As shown in Figure 2, the USP2-CD can be efficiently labeled by the three functional cell-permeable DUB ABPs (**1**, **2**, and **3**), but not the unreactive control probe (**4**). The CPP at the N-terminal region of ubiquitin did not appear to affect the labeling of USP2-CD, as judged by a similar labeling efficiency as the non-CPP-containing counterparts (HA-Ub-PA and HA-Ub-VME). For probes **2** and **3**, we observed a slight smearing of USP2-CD labeling product bands. We attributed this to partial DTT-induced cleavage of the cR_{10}, due to DTT carried over from the USP2-CD stock solution. The reactivity of the DUB ABPs was also evaluated using ubiquitin C-terminal hydrolase 3 (UCHL3), which belongs to a DUB family different from that of USP2 (Figure S1). Similar to USP2-CD labeling, the DUB ABPs **1**, **2**, and **3** labeled UCHL3 with efficiency similar to that of the non-CPP-containing probes (HA-Ub-PA and HA-Ub-VME). Additionally, no labeling of UCHL3 by control probe **4** was observed.

We next compared the cell-lysate DUB labeling using our cell-permeable DUB ABPs to the commonly used HA-Ub-PA and HA-Ub-VME DUB probe (Figure S2). DUB labeling was carried out in HeLa cell lysate as described in the Supporting Information and detected by immunoblotting using an anti-HA antibody. We observed similar labeling efficiency comparing the cell-permeable DUB ABPs (**1**, **2**, and **3**) and HA-Ub-PA/HA-Ub-VME,

indicating that the addition of CPP (TAT or cR_{10}) did not affect the DUB's reactivity toward these Ub-based ABPs. As expected, DUBs labeling was not observed when cell lysate was treated with probe **4**. Considering that the disulfide bond in our cR_{10}-containing cell-permeable DUB ABPs can be reduced in cells, we generated HA-Cys-Ub-PA, HA-Cys-Ub-VME, and HA-Cys-Ub-EA (Schemes S5–S7) probes for comparison to the HA-Ub-PA and HA-Ub-VME probes in the cell-lysate DUB labeling. We observed similar labeling efficiency between HA-Cys-Ub-PA/HA-Cys-Ub-VME and HA-Ub-PA/HA-Ub-VME probes (Figure S3).

Generation of Cell-Permeable Fluorescent Ub-Based DUB ABPs.

To investigate the cell permeability of our Ub-based DUB ABPs, fluorescent cell-permeable DUB ABPs containing either cR_{10} or TAT were generated for live-cell fluorescence confocal microscopy analysis (Figure 3). These fluorescent probes were based on the above-described probe **3**, with a fluorophore tetraethyl-rhodamine (TER) conjugated to the Michael acceptor via click chemistry. We also generated a fluorescent probe that does not harbor a reactive Michael acceptor using a nonreactive linker strategy.[49]

To generate the fluorescent DUB ABPs, we designed and synthesized two linker molecules. The first is a reactive linker pMAL-N_3 ((*E*)-3-(2-(azidomethyl)-1,3-dioxolan-2-yl)prop-2-en-1-amine) that contains a protected Michael acceptor and an azide functional group. pMAL-N_3 was synthesized from (*E*)-2-(3-(2-(bromomethyl)-1,3-dioxolan-2-yl)allyl)-isoindoline-1,3-dione,[23] following reaction with sodium azide and deprotection of phthalimide using hydrazine, with an overall 50% yield (Scheme S8). A protected nonreactive linker pNRL-N_3 (3-(2-(azidomethyl)-1,3-dioxolan-2-yl)propan-1-amine), containing a C–C single bond next to a protected carbonyl group, was synthesized starting from 2-(3-(2-(bromomethyl)-1,3-dioxolan-2-yl)propyl)isoindoline-1,3-dione (Scheme S9). To generate HA-Cys(cR_{10})-Ub-MAL-TER (**5**) (Figure 3a), HA-Cys(TNB)-Ub-MESNA was reacted with an excess amount of pMAL-N_3 to generate HA-Cys(TNB)-Ub-pMAL-N_3, which was then reacted with cR_{10} through disulfide bond exchange reaction to generate HA-Cys(cR_{10})-Ub-pMAL-N_3. HA-Cys(cR_{10})-Ub-pMAL-N_3 was deprotected using TFA/H_2O and *p*-TsOH to activate the Michael acceptor, forming HA-Cys(cR_{10})-Ub-MAL-N_3. In parallel, we synthesized alkyne-modified TER as shown in Scheme S10. HA-Cys(cR_{10})-Ub-MAL-N_3 was then reacted with alkyne-modified TER using click reaction catalyzed by CuBr and TBTA (tris[(1-benzyl-1*H*-1,2,3-triazol-4-yl)methyl]-amine) to generate probe **5**. The product was purified with HPLC, lyophilized, and refolded in MES buffer (50 mM MES, 100 mM NaCl, pH 6.5). The observed mass of 12 547 Da is identical to the calculated molecular weight of 12 547 Da (Figure 3b). Using a method similar to that described above, the nonreactive DUB probe, HA-Cys(cR_{10})-Ub-NRL-TER (**6**), was generated (Scheme S11).

A TAT-containing fluorescent probe TAT-HA-Ub-MAL-TER (**7**) was also generated by reacting TAT-HA-Ub-MESNA with protected Michael acceptor linker (pMAL-N_3), followed by deprotection using TFA/H_2O, *p*-TsOH, and reaction with alkyne-modified TER (Scheme S12). Similarly, TAT-HA-Ub-NRL-TER (**8**) was generated by reacting TAT-HA-Ub-MESNA with pNRL-N_3 followed by deprotection and TER conjugation (Scheme S13). The control

probe HA-Ub-MAL-TER (**9**) was generated similarly, as shown in Scheme S13. SDS-PAGE analysis of the above-described fluorescent DUB ABPs showed good purity (Figure S4). Reactivity of the DUB ABPs was also tested using USP2-CD. As expected, the DUB-reactive fluorescent ABPs (**5**, **7**, and **9**) efficiently labeled USP2-CD (Figure S4). Labeling of USP2-CD was not observed with the nonreactive DUB fluorescent probes (**6** and **8**).

Delivery of Ub-Based DUB ABPs into Cells.

To assess the cellular uptake of the cell-permeable DUB ABPs, we used fluorescence live-cell imaging of the immortalized cervical cancer cell line, HeLa, treated with the cell-permeable fluorescent Ub-based DUB ABPs. HeLa cells were treated with 15 μM of indicated probe for 4 h at 37 °C, 5% CO_2. Post-treatment, cells were rinsed with a trypsin-EDTA solution followed by extensive cold phosphate buffered saline (PBS) wash to remove any remaining probe that was not taken up by the cells. It has been shown previously that trypsin, coupled with extensive wash, removes any noninternalized CPP-linked cargo.[46,50–52] HA-Ub-MAL-TER does not contain a CPP, and therefore is expected to be largely cell impermeable. Therefore, it was used as a negative control.

An increase in TER (red) fluorescence was observed when cells were treated with cR_{10}-containing cell-permeable probes **5** and **6** as compared to those treated with the control probe **9**, which does not contain a CPP (Figure 4). This demonstrates that the addition of cR_{10} to Ub-based DUB ABPs enhances their cell permeability. The presence of the Michael acceptor warhead did not seem to influence the distribution of the cell-permeable probes in cells (comparing **5** and **6**). In parallel, we carried out an imaging experiment using the TAT-containing cell-permeable DUB probes **7** and **8** (Figure 4). Notably, cells treated with DUB ABPs containing the cR_{10} peptide appeared to have a higher abundance of TER fluorescence signal than those treated with DUB ABPs containing the TAT peptide. This observation is in accordance with previous reports that cR_{10} improves cellular uptake of cargo in comparison to TAT.[45,46]

Cell-Permeable Ub-Based DUB ABPs Label DUBs in Live Intact Cells.

Next, we assessed intracellular DUB profiling using the cell-permeable DUB ABPs. HeLa cells were treated with 15 μM probe **2** or HA-Ub-PA for 1 or 4 h at 37 °C and 5% CO_2. HA-Ub-PA was used as a comparison. Post-treatment, cells were rinsed with a trypsin-EDTA solution followed by several cold PBS washes to remove residual ABP not taken up by the cells. Immunoblotting using an anti-HA antibody reveals a number of discrete bands upon cellular treatment of HeLa cells with probe **2** (Figure 5a). The detected bands are indicative of DUB labeling by the ABP.[17,18,20] Few bands were observed in the untreated HeLa cells, or cells treated with HA-Ub-PA. For a comparison, cell lysate-based DUB profiling was also performed. Notably, in the DUB profiling using probe **2**, a clear difference was discernible between live cells and cell lysates despite some common DUB labeling bands. To confirm that no free cell-permeable DUB probes were left over following the trypsin-EDTA solution rinse and PBS buffer wash, we added a highly active DUB UCHL3 to the treated cells following wash to quench any leftover DUB probes if present. The intracellular DUB labeling profiles showed no discernible difference between cells treated with or without UCHL3 (Figure S5). On the other hand, a similar labeling pattern was observed when we

compared the cell lysate labeling of DUBs by probe **2** and HA-Ub-PA (Figure 5a). The treatment time of HeLa cells (1 and 4 h) by the cell-permeable DUB ABP probe **2** did not appear to affect intracellular DUB labeling, as similar labeling pattern and band intensity were observed. This indicates that the uptake of the cR_{10}-containing cell-permeable DUB ABP was fast, and reached a concentration effective to label the intracellular DUBs in 1 h or less.

In addition to intracellular DUB profiling, individual DUBs (USP15 and USP7) were selected for immunoblotting using the DUB-specific antibodies, whereas GAPDH served as a loading control. USP15 and USP7 were robustly labeled when HeLa cells were treated with 15 μM probe **2** for 4 h at 37 °C and 5% CO_2 as shown in Figure 5b. DUB labeling is indicated by the appearance of a higher molecular weight band, which is absent in the untreated control.

We then sought to investigate intracellular profiling of DUB using the VME-containing cell-permeable probe **3**. Similar to HA-Cys(cR_{10})-Ub-PA (**2**), DUB labeling was observed when HeLa cells were treated with probe **3**, but not with HA-Ub-VME (Figure S6a). Unlike cells treated with probe **2**, time-dependent DUB labeling was observed for probe **3**. Prolonged incubation (4 h) of the HeLa cells with probe **3** resulted in increased band intensity. We also noticed a difference in the labeling pattern by probe **3** as compared to probe **2** and some smearing when probe **3** was used in intracellular labeling. It could be due to different reactivity of the warheads and susceptibility to intracellular thiol-containing molecules. Intracellular labeling of specific DUBs by probe **3** was also accessed by immunoblotting using DUB-specific antibodies. Robust labeling of USP15 and USP7 was observed when cells were treated with probe **3** (Figure S6b).

Lastly, intracellular DUB profiling by 15 μM TAT-HA-Ub-PA (probe **1**) was investigated by immunoblotting. Clear DUB labeling was seen (Figure S7a), as observed for probes **2** and **3**. An absence of DUB labeling was observed when cells were treated with HA-Ub-PA. Using DUB-specific antibodies, the labeling of USP15 and USP7 in HeLa cells by probe **1** or HA-Ub-PA was examined. Treatment of cells with probe **1** led to labeling of USP15 and USP7, but not by HA-Ub-PA (Figure S7b).

To directly compare the effectiveness of the DUB ABPs in intracellular DUB labeling, we evaluated the cell-permeable DUB ABPs in parallel on the same immunoblot. In agreement with the observations described above, cells treated with HAUb-PA and HA-Ub-VME showed little labeling (Figure 5c). Few DUB labeling bands were observed when cells were treated with probe **4**. Notably, the cell-permeable DUB probes **2** and **3** showed an increased number of labeling bands as compared to probe **1**, which could be due to a difference in the probe transduction efficiency.

Cell-Permeable Ub-Based DUB ABPs in Evaluating Intracellular Activity of DUB Inhibitors.

DUB profiling with ABPs is often utilized in DUB inhibitor discovery. Currently, the assessment has been largely limited to cell lysates because the existing Ub-based DUB ABPs cannot effectively penetrate the cell membrane. With the cell-permeable DUB ABPs in hand, we sought to demonstrate the utility of the newly developed DUB ABP in inhibitor

discovery. As a proof of concept, we chose PR-619, a widely used pan-DUB inhibitor, that has been shown to be cell-permeable.[10] HeLa cells were pretreated with 5, 25, or 50 μM of PR-619, or an equivalent volume of DMSO, for 2 h at 37 °C and 5% CO_2. The cells were then treated with 15 μM probe **2** in the presence of PR-619 for another hour. Cells were then rinsed with a trypsin-EDTA solution, followed by several cold PBS washes to remove untransduced probe. For comparison, DUB profiling in cell lysate in the presence of PR-619 was also performed. Labeled DUBs were visualized by immunoblotting, and GAPDH served as the loading control. Treatment of HeLa cells with high concentrations of PR-619 (50 μM) led to reduced intensity in many labeled DUB bands, indicating intracellular inhibition of DUB activity by PR-619 (Figure 6). Notably, inhibition of DUB activities by PR-619 in the cell lysate-based experiment is more pronounced than that in the cell-based experiment. The difference observed in cell lysate and intact cells could be due to a number of reasons. The most likely cause is the membrane permeability of compound or its tendency to be depleted or trapped by cellular components. This emphasizes the importance of evaluating the potency of DUB inhibitors in a physiologically relevant condition by using cell-permeable DUB probes.

Proteome-Wide DUB Profiling Using Cell-Permeable Probes.

To identify the DUBs captured by the cell-permeable DUB ABP, we performed intracellular proteome-wide DUB profiling using label-free quantitative (LFQ) mass spectrometry. LFQ MS analysis enables a comparison of relative protein abundance between complex samples.[29,30,53,54] Anti-HA beads were used to enrich the proteins captured by the cell-permeable DUB probe. After elution with a 50 mM NaOH solution, proteins were trypsin digested, and subjected to LC–MS/MS analysis using Orbitrap Q-Exactive mass spectrometer. Raw data sets were processed using MaxQuant to search against the human proteome with the built-in Andromeda engine.[55–58] The MaxLFQ module within MaxQuant was used to quantify relative protein intensity among the pulldown experiments, which corresponded to cellular treatment using probe **2**, HA-Ub-PA probe, or beads control, respectively.

Identified DUBs, E3's, and E2's, and their corresponding LFQ intensity scores are listed in Tables S1 and S2, respectively. 34 DUBs, 21 E3's, and 2 E2's were identified at least once in any of the pulldowns, while others are largely housekeeping proteins. The identified DUBs belong to four out of the five families of cysteine protease DUBs (24 USPs, 6 OTUs, 3 UCHs, and 1 MJD). The MaxQuant output was first visualized using a heat map to identify enriched protein groups (Figure 7a). Red indicates that the protein group is enriched (higher LFQ intensity score), while blue indicates a weak enrichment (lower LFQ intensity score). Two clusters of proteins were enriched in samples treated with probe **2** as compared to the beads control or HA-Ub-PA treated cells. One of these clusters corresponds to the DUBs, E2's, and E3's. The inset in Figure 7a shows the DUBs within the cluster. The second cluster was comprised of protein groups corresponding to subunits of the 26S proteasome (PSMC1, PSMC2, PSMC3, PSMC4, PSMC5, PSMC6, PSMD1, PSMD2, PSMD3, PSMD5, PSMD6, PSMD7, PSMD10, PSMD11, PSMD12, PSMD13, and PSMD14). USP14 and UCHL5 (also known as UCH37), captured by probe **2**, are proteasome associated DUBs,[59,60] which could account for the observed enrichment of proteasomal subunits.

Next, a two-sample *t* test was performed to obtain *p*-values of difference (fold change) in LFQ intensity scores between two paired pulldown experiments. A volcano plot, or scatterplot, was generated by graphing the *p*-values ($-\log_{10}$) on the *y*-axis, and the fold difference of the average LFQ intensities of the paired samples, represented as $\log_2$, on the *x*-axis. Protein groups with a fold difference of 2 or greater and a *p*-value < 0.05 were deemed significant. These cutoffs are commonly accepted in similar studies.[29,30] Comparison of samples generated from cells treated with probe **2** to samples generated from cells treated with HA-Ub-PA revealed that 27 DUBs and 3 E3's were significantly enriched by probe **2** (Figure 7b). Next, we analyzed cells treated with probe **2** as compared to the beads control and found 27 DUBs, 3 E3's, and 1 E2 were significantly enriched (Figure S8a). Comparison of cells treated with HA-Ub-PA to beads control revealed no significant enrichment of any DUBs, E2's, or E3's (Figure S8b). As a comparison, intracellular proteome-wide DUB profiling using HA-Cys(cR_{10})-EA (**4**) was also performed. Among the protein identified, only 2 DUBs (UCHL3 and USP42) were reliably captured by probe **4**, likely through noncovalent binding, but with low LFQ values (Table S1). A pairwise analysis comparing cells treated with 15 μM probe **2** and probe **4** identified 26 DUBs and 3 E3's, significantly enriched by **2** (Figure S9).

We carried out intracellular proteome-wide DUB profiling using 15 μM TAT-HA-Ub-PA (**1**). The protein groups pulled out by probe **1** were shown as heatmap (Figure S10). Identified DUBs, E3's, and E2's, and their corresponding LFQ intensity scores are listed in Tables S3 and S4, respectively. In comparison of sample treated with probe **1** to the beads control, 30 DUBs, 6 E3's and 2 E2's were significantly enriched by TAT-HA-Ub-PA (**1**) (Figure S11). Comparing the DUBs captured by probes **1** and **2**, we found interesting differences despite that many overlapping DUBs were captured by the two probes. CYLD, OTUD3, UCHL3, USP34, and USP35 were captured exclusively by probe **1**, while USP32, USP33, and USP37 were exclusively captured by probe **2** (Figure S12). Among the 5 DUBs exclusively pulled down by probe **1**, 3 of them are predominantly localized in nucleus (CYLD, USP34, USP35) according to the Human Protein Atlas (www.proteinatlas.org).[61]

Next, we compared intracellular DUB labeling by probes **1** and **2** at reduced probe concentrations in the cell culture. We treated HeLa cells with 1, 5, and 10 μM of probe **1** and probe **2**, respectively. We then performed intracellular proteome-wide DUB profiling using label-free quantitative (LFQ) mass spectrometry for different concentrations of cell-permeable probes. The LFQ values of DUBs and ligases are listed in Table S5. For both probes, a higher concentration of probe **1** or **2** (10 μM) captured more DUBs than did a lower concentration of probe (1 and 5 μM). Importantly, for the same probe concentration at 5 and 10 μM, probe **2** captured more DUBs than did probe **1**. For the DUBs pulled down by both probes, the LFQ score of probe **2** is substantially higher than that of probe **1**. Our results indicate that probe **2** was more efficient in capturing cellular DUBs.

We also performed HeLa cell lysate DUB profiling using probe **2** to assess the potential difference in the identification of DUBs in live cells versus cell lysate. Ten DUBs were identified using MS-based LFQ analysis in cell lysate (Table S6). All 10 DUBs (ATXN3, USP10, USP14, USP15, USP24, USP7, USP8, USP19, UCHL5, and OTUB1) identified

specifically in our cell lysate profiling experiment were also identified in the intracellular DUB profiling experiment. However, 17 additional DUBs (OTUD4, USP47, USP9X, OTUD5, USP48, USP5, VCPIP1, USP16, OTUD6B, USP3, USP28, USP33, OTUD7B, USP36, BAP1, USP32, and USP4) were identified in the intracellular DUB profiling experiment.

Additionally, DUBs are known to localize to different organelles and locations in cells.[61,62] Remarkably, the DUBs that we identified intracellularly by the cell-permeable probe **2** are known to be associated with different cell organelles according to the Human Protein Atlas. For example, ATXN3, BAP1, OTUD7B, UCHL5, USP28, USP3, USP36, and USP7 are predominantly located in the nucleus. Meanwhile, OTUB1, OTUD4, OTUD5, USP14, USP15, and USP9X are located predominantly in the cytoplasm. OTUD6B, USP10, USP16, USP24, USP48, and USP5 are found in both cytoplasm and nucleus, while USP32, USP33, USP8, and VCPIP1 reside predominantly in the Golgi apparatus. USP47 is mainly located within the cytoskeleton (intermediate filaments), and USP19 is predominantly found within the membrane of the endoplasmic reticulum. Cellular locations of DUBs were determined using the Human Protein Atlas. To confirm probe **2** can label DUBs in both cytoplasm and nucleus, we separated the cytoplasmic and nuclear fractions after lysing the probe-treated cells. Western blotting using anti-GAPDH and Lamin A/C showed effective separation of cytoplasmic and nuclear fractions (Figure S13). Using label-free quantitative (LFQ) mass spectrometry, we identified DUBs predominantly in cytoplasm (OTUD4, OTUD6B, USP15, USP24) and nucleus (BAP1, USP36, USP7) in the respective cytoplasmic and nuclear fractions (Tables S7 and S8). Collectively, our results demonstrate the robustness and advantage of intracellular DUB profiling using the cell-permeable Ub-based DUB ABPs.

CONCLUSIONS

A better understanding of DUB cellular functions and regulations require cell-permeable activity-based DUB probes. We report the development and implementation of cell-permeable ubiquitin-based DUB ABPs to investigate DUB activity in intact cells. This was made feasible through the usage of CPPs. While TAT was expressed as a linear fusion to the N-terminus of Ub, a cyclic polyarginine CPP was linked to Ub via a disulfide bond. The advantage of using disulfide tethering is the release of the cR_{10} peptide upon cellular entry. Using live-cell imaging, we demonstrated efficient cellular uptake of fluorescently labeled cell-permeable DUB ABPs. We also observed higher cellular uptake for the cR_{10}-containing DUB ABPs than for the TAT-tagged DUB ABPs. Immunoblotting analysis using an anti-HA antibody demonstrated intracellular labeling of DUBs by probes **1**, **2**, and **3** in human HeLa cells. Our results indicate that the cR_{10}-containing probes **2** and **3** are more efficient ABPs in intracellular DUB profiling than the TAT-containing probe **1**. This was evidenced by a larger number of bands detected and an overall higher intensity of the labeled DUB bands. We attributed this to the more efficient cellular transduction of the probes. Additionally, intracellular labeling of the specific DUBs, USP15 and USP7, by the cell-permeable Ub-based DUB ABPs was also observed. Using a pan-DUB inhibitor PR-619, we demonstrated that the cell-permeable DUB ABPs are amenable for assessing the inhibition of DUBs in live cells by small-molecule inhibitors. Moreover, our novel cell-permeable DUB ABP can be used in conjunction with MS-based LFQ analysis to achieve proteome-wide DUB

profiling in intact cells. In comparison to our cell lysate-based DUB profiling experiment, a larger number of DUBs was significantly enriched in the intracellular DUB profiling, and the identified DUBs are associated with different cell organelles. Collectively, our study suggests an advantage of carrying out DUB profiling in live, intact cells.

The cell-permeable DUB ABPs described in this work will allow a thorough investigation into the activity of DUBs located within intact cellular organelles. This will greatly advance our understanding of DUB function and regulation under physiological conditions. Additionally, these new ABPs can be used to interrogate DUB activities within live cells in response to intracellular and extracellular stimuli in a range of cellular pathways including cell cycle regulation, DNA damage repair, TGF-β signaling, and antiviral response. This will advance our knowledge of the dynamic regulation of DUB activity in cells. Also, the cell-permeable DUB ABP can be combined with the AlphaLISA DUB assay that we previously developed[14] to achieve a cell-based DUB assay amenable for high-throughput screening and DUB inhibitor discovery. We expect that this strategy could be readily expanded to enable cellular profiling of deISGylases, deNeddylases, deSUMOylases, and a subset of ubiquitin ligases and ubiquitin-conjugating enzymes. Adding to the fast-expanding toolbox of DUB research, our cell-permeable Ub-based DUB ABPs will help to shed new light on the diverse biological roles that DUBs play in cells and propel the future development of DUB inhibitors.

Supplementary Material

Refer to Web version on PubMed Central for supplementary material.

ACKNOWLEDGMENTS

This work was supported in part by U.S. National Institutes of Health grants R01GM097468 and R21NS085509 to Z.Z. Special thanks go to Drs. PapaNii Asare-Okai and Zhihua Yang in the Mass Spectrometry Facility at the University of Delaware for their help in the proteomics data collection and valuable insights offered for data processing. Additionally, this work was made possible by the Delaware COBRE program, supported by a grant from the National Institute of General Medical Sciences — NIGMS (5 P30 GM110758-02) from the National Institutes of Health. We also thank Michael Moore and Dr. Jeffery Caplan in the Bioimaging Center for assistance and conversations associated with live-cell imaging experiments. Additionally, microscopy access was supported by grants from the NIH-NIGMS (P20 GM103446), the National Science Foundation (IIA-1301765), and the State of Delaware.

REFERENCES

(1). Ikeda F; Crosetto N; Dikic I Cell 2010, 143 (5), 677–81. [PubMed: 21111228]

(2). Harrigan JA; Jacq X; Martin NM; Jackson SP Nat. Rev. Drug Discovery 2018, 17 (1), 57–78. [PubMed: 28959952]

(3). Lee BH; Lee MJ; Park S; Oh DC; Elsasser S; Chen PC; Gartner C; Dimova N; Hanna J; Gygi SP; Wilson SM; King RW; Finley D Nature 2010, 467 (7312), 179–84. [PubMed: 20829789]

(4). Kapuria V; Peterson LF; Fang D; Bornmann WG; Talpaz M; Donato NJ Cancer Res. 2010, 70 (22), 9265–76. [PubMed: 21045142]

(5). D'Arcy P; Brnjic S; Olofsson MH; Fryknas M; Lindsten K; De Cesare M; Perego P; Sadeghi B; Hassan M; Larsson R; Linder S Nat. Med 2011, 17 (12), 1636–40. [PubMed: 22057347]

(6). Liang Q; Dexheimer TS; Zhang P; Rosenthal AS; Villamil MA; You C; Zhang Q; Chen J; Ott CA; Sun H; Luci DK; Yuan B; Simeonov A; Jadhav A; Xiao H; Wang Y; Maloney DJ; Zhuang Z Nat. Chem. Biol 2014, 10 (4), 298–304. [PubMed: 24531842]

(7). Kategaya L; Di Lello P; Rougé L; Pastor R; Clark KR; Drummond J; Kleinheinz T; Lin E; Upton JP; Prakash S; Heideker J; McCleland M; Ritorto MS; Alessi DR; Trost M; Bainbridge TW; Kwok MCM; Ma TP; Stiffler Z; Brasher B; Tang Y; Jaishankar P; Hearn BR; Renslo AR; Arkin MR; Cohen F; Yu K; Peale F; Gnad F; Chang MT; Klijn C; Blackwood E; Martin SE; Forrest WF; Ernst JA; Ndubaku C; Wang X; Beresini MH; Tsui V; Schwerdtfeger C; Blake RA; Murray J; Maurer T; Wertz IE Nature 2017, 550 (7677), 534–538. [PubMed: 29045385]

(8). Turnbull AP; Ioannidis S; Krajewski WW; Pinto-Fernandez A; Heride C; Martin ACL; Tonkin LM; Townsend EC; Buker SM; Lancia DR; Caravella JA; Toms AV; Charlton TM; Lahdenranta J; Wilker E; Follows BC; Evans NJ; Stead L; Alli C; Zarayskiy VV; Talbot AC; Buckmelter AJ; Wang M; McKinnon CL; Saab F; McGouran JF; Century H; Gersch M; Pittman MS; Marshall CG; Raynham TM; Simcox M; Stewart LMD; McLoughlin SB; Escobedo JA; Bair KW; Dinsmore CJ; Hammonds TR; Kim S; Urbé S; Clague MJ; Kessler BM; Komander D Nature 2017, 550 (7677), 481–486. [PubMed: 29045389]

(9). Colland F; Formstecher E; Jacq X; Reverdy C; Planquette C; Conrath S; Trouplin V; Bianchi J; Aushev VN; Camonis J; Calabrese A; Borg-Capra C; Sippl W; Collura V; Boissy G; Rain JC; Guedat P; Delansorne R; Daviet L Mol. Cancer Ther 2009, 8 (8), 2286–95. [PubMed: 19671755]

(10). Altun M; Kramer HB; Willems LI; McDermott JL; Leach CA; Goldenberg SJ; Kumar KG; Konietzny R; Fischer R; Kogan E; Mackeen MM; McGouran J; Khoronenkova SV; Parsons JL; Dianov GL; Nicholson B; Kessler BM Chem. Biol 2011, 18 (11), 1401–12. [PubMed: 22118674]

(11). Mistry H; Hsieh G; Buhrlage SJ; Huang M; Park E; Cuny GD; Galinsky I; Stone RM; Gray NS; D'Andrea AD; Parmar K Mol. Cancer Ther 2013, 12 (12), 2651–62. [PubMed: 24130053]

(12). Yue W; Chen Z; Liu H; Yan C; Chen M; Feng D; Wu H; Du L; Wang Y; Liu J; Huang X; Xia L; Liu L; Wang X; Jin H; Wang J; Song Z; Hao X; Chen Q Cell Res. 2014, 24 (4), 482–96. [PubMed: 24513856]

(13). Davis MI; Pragani R; Fox JT; Shen M; Parmar K; Gaudiano EF; Liu L; Tanega C; McGee L; Hall MD; McKnight C; Shinn P; Nelson H; Chattopadhyay D; D'Andrea AD; Auld DS; DeLucas LJ; Li Z; Boxer MB; Simeonov AJ Biol. Chem 2016, 291 (47), 24628–24640.

(14). Ott CA; Baljinnyam B; Zakharov AV; Jadhav A; Simeonov A; Zhuang Z ACS Chem. Biol 2017, 12 (9), 2399–2407. [PubMed: 28836754]

(15). Peterson LF; Sun H; Liu Y; Potu H; Kandarpa M; Ermann M; Courtney SM; Young M; Showalter HD; Sun D; Jakubowiak A; Malek SN; Talpaz M; Donato NJ Blood 2015, 125 (23), 3588–97. [PubMed: 25814533]

(16). Tian Z; D'Arcy P; Wang X; Ray A; Tai YT; Hu Y; Carrasco RD; Richardson P; Linder S; Chauhan D; Anderson KC Blood 2014, 123 (5), 706–16. [PubMed: 24319254]

(17). Borodovsky A; Kessler BM; Casagrande R; Overkleeft HS; Wilkinson KD; Ploegh HL EMBO J. 2001, 20 (18), 5187–96. [PubMed: 11566882]

(18). Borodovsky A; Ovaa H; Kolli N; Gan-Erdene T; Wilkinson KD; Ploegh HL; Kessler BM Chem. Biol 2002, 9 (10), 1149–59. [PubMed: 12401499]

(19). de Jong A; Merkx R; Berlin I; Rodenko B; Wijdeven RH; El Atmioui D; Yalcin Z; Robson CN; Neefjes JJ; Ovaa H ChemBioChem 2012, 13 (15), 2251–8. [PubMed: 23011887]

(20). Ekkebus R; van Kasteren SI; Kulathu Y; Scholten A; Berlin I; Geurink PP; de Jong A; Goerdayal S; Neefjes J; Heck AJ; Komander D; Ovaa HJ Am. Chem. Soc 2013, 135 (8), 2867–70.

(21). de Jong A; Witting K; Kooij R; Flierman D; Ovaa H Angew. Chem., Int. Ed 2017, 56 (42), 12967–12970.

(22). McGouran JF; Gaertner SR; Altun M; Kramer HB; Kessler BM Chem. Biol 2013, 20 (12), 1447–55. [PubMed: 24290882]

(23). Li G; Liang Q; Gong P; Tencer AH; Zhuang Z Chem. Commun. (Cambridge, U. K.) 2014, 50 (2), 216–8.

(24). Haj-Yahya N; Hemantha HP; Meledin R; Bondalapati S; Seenaiah M; Brik A Org. Lett 2014, 16 (2), 540–3. [PubMed: 24364494]

(25). Mulder MP; El Oualid F; ter Beek J; Ovaa H ChemBioChem 2014, 15 (7), 946–9. [PubMed: 24623714]

(26). Flierman D; van der Heden van Noort GJ; Ekkebus R; Geurink PP; Mevissen TE; Hospenthal MK; Komander D; Ovaa H Cell Chem. Biol 2016, 23 (4), 472–82. [PubMed: 27066941]

(27). Liang J; Zhang L; Tan XL; Qi YK; Feng S; Deng H; Yan Y; Zheng JS; Liu L; Tian CL Angew. Chem., Int. Ed 2017, 56 (10), 2744–2748.

(28). Tan XD; Pan M; Gao S; Zheng Y; Shi J; Li YM Chem. Commun. (Cambridge, U. K.) 2017, 53 (73), 10208–10211.

(29). Zhang X; Smits AH; van Tilburg GB; Jansen PW; Makowski MM; Ovaa H; Vermeulen M Mol. Cell 2017, 65 (5), 941–955.e8. [PubMed: 28190767]

(30). Zhang X; Smits AH; van Tilburg GB; Ovaa H; Huber W; Vermeulen M Nat. Protoc 2018, 13 (3), 530–550. [PubMed: 29446774]

(31). Meledin R; Mali SM; Kleifeld O; Brik A Angew. Chem., Int. Ed 2018, 57 (20), 5645–5649.

(32). Gong P; Davidson GA; Gui W; Yang K; Bozza WP; Zhuang Z Chemical science 2018, DOI: 10.1039/C8SC01573B.

(33). Hewings DS; Heideker J; Ma TP; AhYoung AP; El Oualid F; Amore A; Costakes GT; Kirchhofer D; Brasher B; Pillow T; Popovych N; Maurer T; Schwerdtfeger C; Forrest WF; Yu K; Flygare J; Bogyo M; Wertz IE Nat. Commun 2018, 9 (1), 1162. [PubMed: 29563501]

(34). Boudreaux DA; Maiti TK; Davies CW; Das C Proc. Natl. Acad. Sci. U. S. A 2010, 107 (20), 9117–22. [PubMed: 20439756]

(35). Sheedlo MJ; Qiu J; Tan Y; Paul LN; Luo ZQ; Das C Proc. Natl. Acad. Sci. U. S. A 2015, 112 (49), 15090–5. [PubMed: 26598703]

(36). Bekes M; van der Heden van Noort GJ; Ekkebus R; Ovaa H; Huang TT; Lima CD Mol. Cell 2016, 62 (4), 572–85. [PubMed: 27203180]

(37). Mevissen TET; Kulathu Y; Mulder MPC; Geurink PP; Maslen SL; Gersch M; Elliott PR; Burke JE; van Tol BDM; Akutsu M; Oualid FE; Kawasaki M; Freund SMV; Ovaa H; Komander D Nature 2016, 538 (7625), 402–405. [PubMed: 27732584]

(38). Weber A; Elliott PR; Pinto-Fernandez A; Bonham S; Kessler BM; Komander D; El Oualid F; Krappmann D Cell Chem. Biol 2017, 24 (10), 1299–1313 e7. [PubMed: 28919039]

(39). Abdul Rehman SA; Kristariyanto YA; Choi SY; Nkosi PJ; Weidlich S; Labib K; Hofmann K; Kulathu Y Mol. Cell 2016, 63 (1), 146–55. [PubMed: 27292798]

(40). Claessen JHL; Witte MD; Yoder NC; Zhu AY; Spooner E; Ploegh HL ChemBioChem 2013, 14 (3), 343–52. [PubMed: 23335262]

(41). Ward JA; McLellan L; Stockley M; Gibson KR; Whitlock GA; Knights C; Harrigan JA; Jacq X; Tate EW ACS Chem. Biol 2016, 11 (12), 3268–3272. [PubMed: 27779380]

(42). Mulder MP; Witting K; Berlin I; Pruneda JN; Wu KP; Chang JG; Merkx R; Bialas J; Groettrup M; Vertegaal AC; Schulman BA; Komander D; Neefjes J; El Oualid F; Ovaa H Nat. Chem. Biol 2016, 12 (7), 523–30. [PubMed: 27182664]

(43). Raucher D; Ryu JS Trends Mol. Med 2015, 21 (9), 560–70. [PubMed: 26186888]

(44). Lättig-Tünnemann G; Prinz M; Hoffmann D; Behlke J; Palm-Apergi C; Morano I; Herce HD; Cardoso MC Nat. Commun 2011, 2, 453. [PubMed: 21878907]

(45). Nischan N; Herce HD; Natale F; Bohlke N; Budisa N; Cardoso MC; Hackenberger CP Angew. Chem., Int. Ed 2015, 54 (6), 1950–3.

(46). Herce HD; Schumacher D; Schneider AFL; Ludwig AK; Mann FA; Fillies M; Kasper MA; Reinke S; Krause E; Leonhardt H; Cardoso MC; Hackenberger CP R. Nat. Chem 2017, 9 (8), 762–771.

(47). Herce HD; Garcia AE; Cardoso MC J. Am. Chem. Soc 2014, 136 (50), 17459–67. [PubMed: 25405895]

(48). Saito G; Swanson JA; Lee KD Adv. Drug Delivery Rev 2003, 55 (2), 199–215.

(49). Yang K; Li G; Gong P; Gui W; Yuan L; Zhuang Z ChemBioChem 2016, 17 (11), 995–8. [PubMed: 27113245]

(50). Richard JP; Melikov K; Vives E; Ramos C; Verbeure B; Gait MJ; Chernomordik LV; Lebleu BJ Biol. Chem 2003, 278 (1), 585–90.

(51). Mäe M; Myrberg H; Jiang Y; Paves H; Valkna A; Langel U Biochim. Biophys. Acta, Biomembr 2005, 1669 (2), 101–7.

(52). Yukawa H; Noguchi H; Nakase I; Miyamoto Y; Oishi K; Hamajima N; Futaki S; Hayashi S Cell Transplant 2010, 19 (6), 901–9. [PubMed: 20587149]

(53). Spruijt CG; Gnerlich F; Smits AH; Pfaffeneder T; Jansen PW; Bauer C; Münzel M; Wagner M; Müller M; Khan F; Eberl HC; Mensinga A; Brinkman AB; Lephikov K; Müller U; Walter J; Boelens R; van Ingen H; Leonhardt H; Carell T; Vermeulen M Cell 2013, 152 (5), 1146–59. [PubMed: 23434322]

(54). Chen Y; Wang F; Xu F; Yang T Adv. Exp. Med. Biol 2016, 919, 255–279. [PubMed: 27975224]

(55). Cox J; Neuhauser N; Michalski A; Scheltema RA; Olsen JV; Mann MJ Proteome Res. 2011, 10 (4), 1794–805.

(56). Cox J; Hein MY; Luber CA; Paron I; Nagaraj N; Mann M Mol. Cell. Proteomics 2014, 13 (9), 2513–26. [PubMed: 24942700]

(57). Cox J; Mann M Nat. Biotechnol 2008, 26 (12), 1367–72. [PubMed: 19029910]

(58). Tyanova S; Temu T; Cox J Nat. Protoc 2016, 11 (12), 2301–2319. [PubMed: 27809316]

(59). Guterman A; Glickman MH Curr. Protein Pept. Sci 2004, 5 (3), 201–11. [PubMed: 15188770]

(60). Lee MJ; Lee BH; Hanna J; King RW; Finley D Mol. Cell. Proteomics 2011, 10 (5), R110 003871.

(61). Thul PJ; Åkesson L; Wiking M; Mahdessian D; Geladaki A; Ait Blal H; Alm T; Asplund A; Björk L; Breckels LM; Bäckström A; Danielsson F; Fagerberg L; Fall J; Gatto L; Gnann C; Hober S; Hjelmare M; Johansson F; Lee S; Lindskog C; Mulder J; Mulvey CM; Nilsson P; Oksvold P; Rockberg J; Schutten R; Schwenk JM; Sivertsson Å; Sjöstedt E; Skogs M; Stadler C; Sullivan DP; Tegel H; Winsnes C; Zhang C; Zwahlen M; Mardinoglu A; Pontén F; von Feilitzen K; Lilley KS; Uhlén M; Lundberg E Science 2017, 356 (6340), eaal3321. [PubMed: 28495876]

(62). Urbé S; Liu H; Hayes SD; Heride C; Rigden DJ; Clague MJ Mol. Biol. Cell 2012, 23 (6), 1095–103. [PubMed: 22298430]

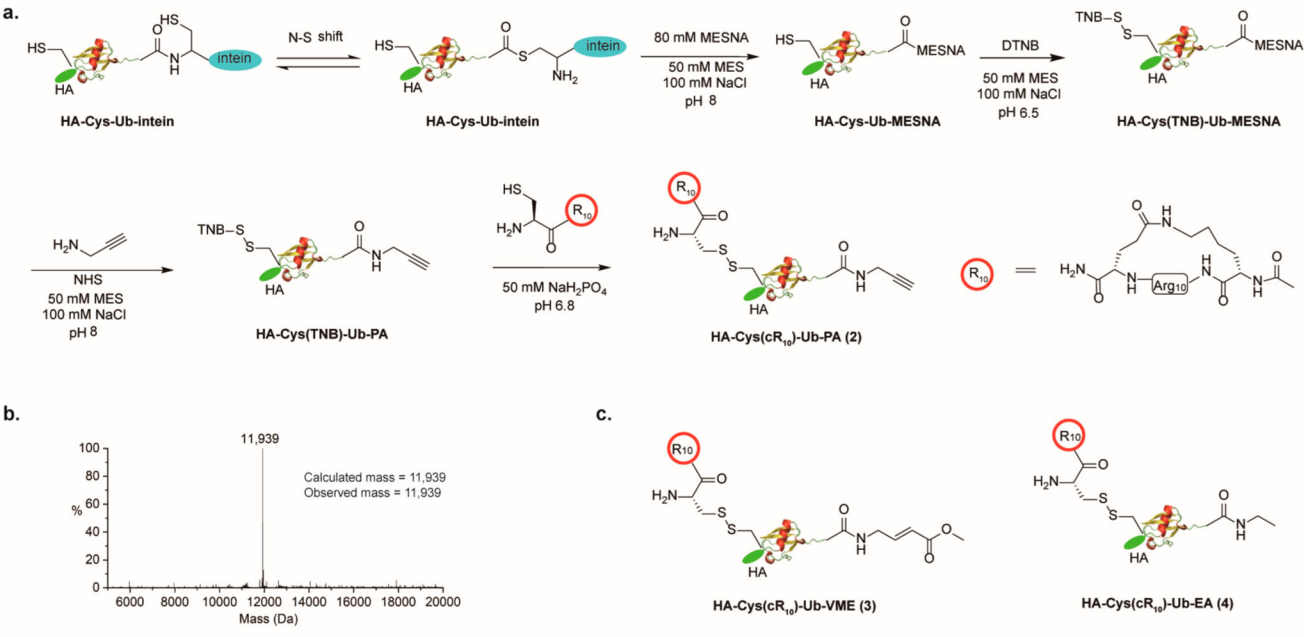

Figure 1.

Generation of cR_{10}-containing cell-permeable DUB ABPs. (a) Chemical steps of generating cell-permeable HA-Cys(cR_{10})-Ub-PA (**2**) probe. (b) ESI–MS characterization of probe **2**. (c) Structure of cell-permeable probe HA-Cys(cR_{10})-Ub-VME (**3**) and HA-Cys(cR_{10})-Ub-EA (**4**).

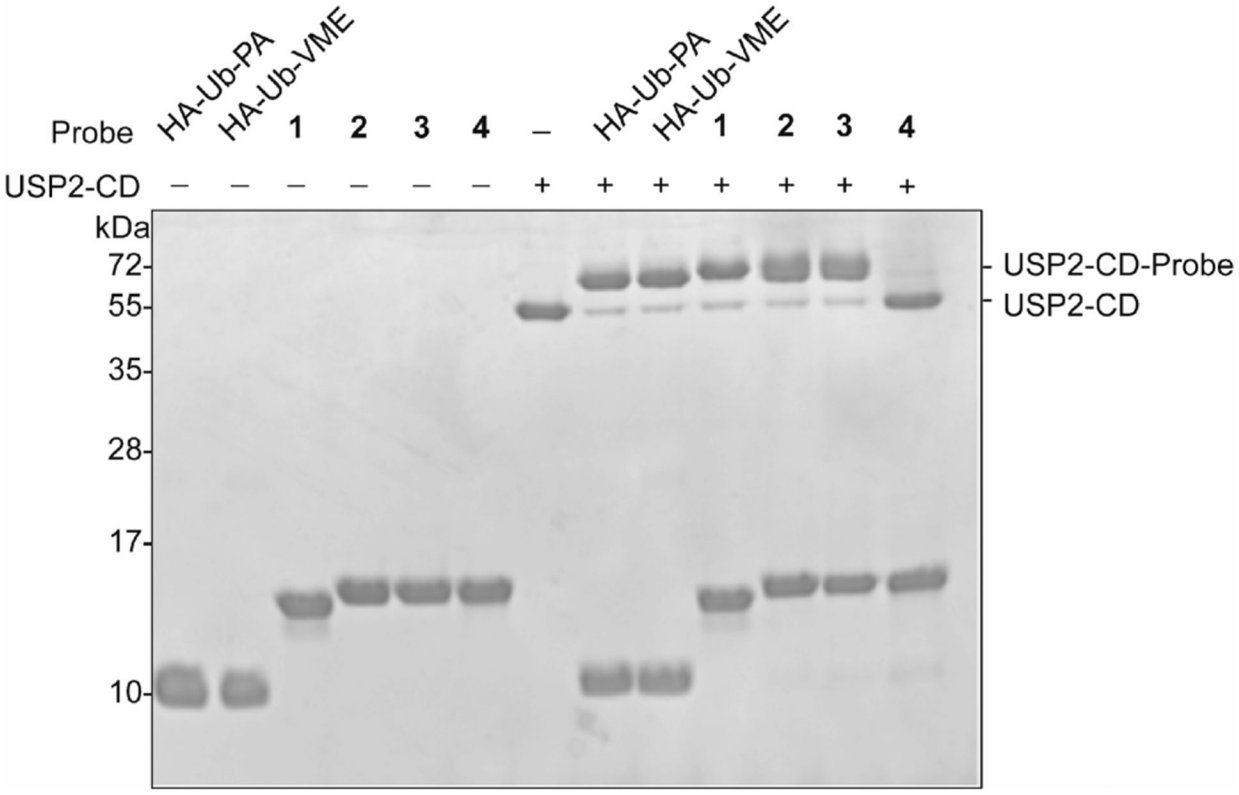

Figure 2.

Labeling of USP2-CD by DUB probes **1**, **2**, and **3** as compared to the control probe **4**. The labeling reaction products were resolved on a 20% SDS-PAGE gel and analyzed using Coomassie brilliant blue staining.

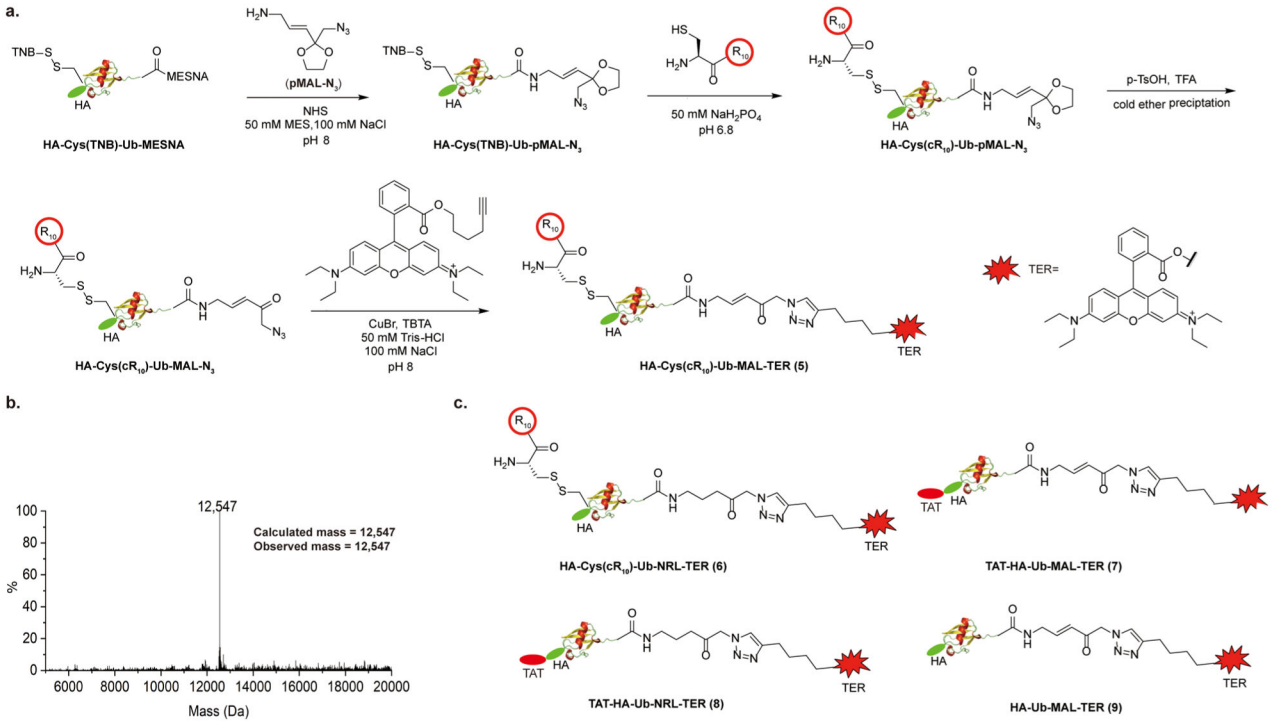

Figure 3.

Generation of cR_{10} containing cell-permeable fluorescent probes and ESI–MS characterization of HA-Cys(cR_{10})-Ub-MAL-TER (**5**). (a) Scheme illustrating the generation of HA-Cys(cR_{10})-Ub-MAL-TER (**5**). (b) ESI–MS characterization of cell-permeable fluorescent probe HA-Cys(cR_{10})-Ub-MAL-TER (**5**). (c) Structure of cell-permeable fluorescent probes HA-Cys(cR_{10})-Ub-NRL-TER (**6**), TAT-HA-Ub-MAL-TER (**7**), TAT-HA-Ub-NRL-TER (**8**), and HA-Ub-MAL-TER (**9**).

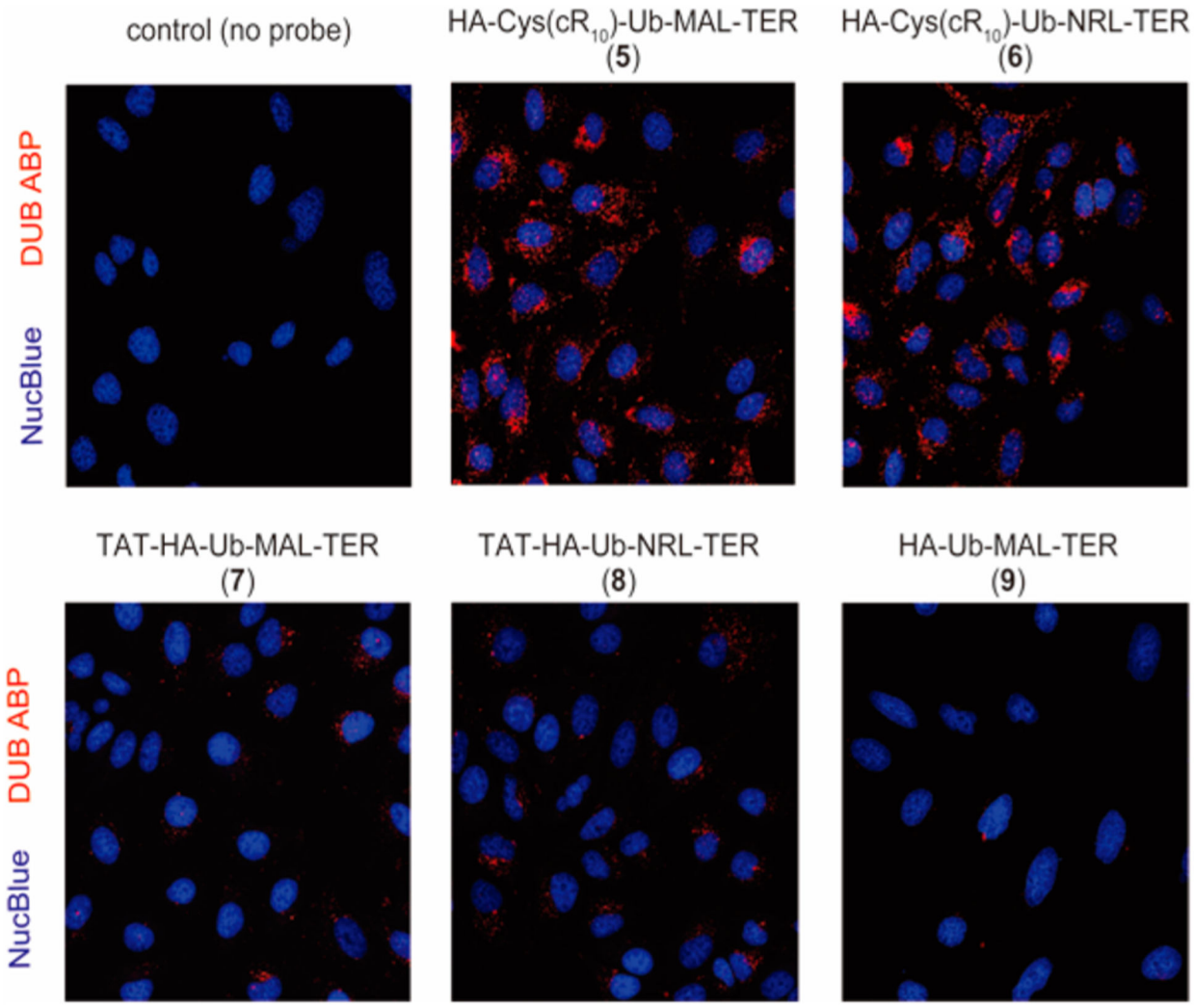

Figure 4.

Live-cell fluorescence imaging of HeLa cells treated with the cell-permeable fluorescent Ub-based DUB ABPs. Comparison of HeLa cells treated with indicated probes **5**, **6**, **7**, **8**, and **9** (15 μM, 4 h). DUB ABPs are visualized using TER fluorescence (red channel), and NucBlue Live Readyprobes Reagent was utilized for nuclear staining (blue channel).

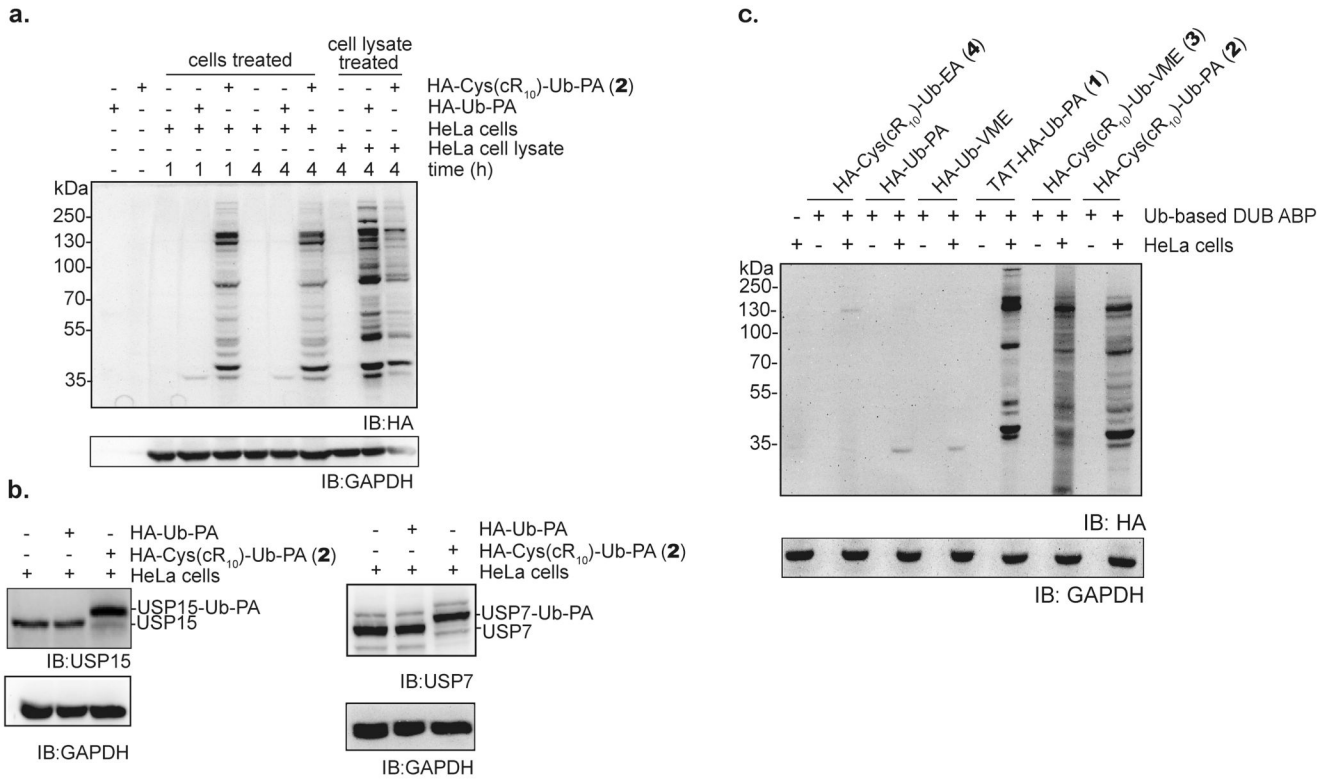

Figure 5.

Intracellular DUB profiling using cell-permeable DUB ABPs. (a) DUB profiling in HeLa cells using HA-Cys(cR_{10})-Ub-PA (**2**) or HA-Ub-PA at 15 μM for 1 and 4 h. Profiling of DUBs in HeLa cell lysate using HA-Cys(cR_{10})-Ub-PA (**2**) and HA-Ub-PA (4 h, 15 μM) is also shown for comparison. (b) Intracellular labeling of USP15 and USP7 using HA-Cys(cR_{10})-Ub-PA (**2**) or HA-Ub-PA for 4 h at 15 μM. (c) Comparison of intracellular DUB labeling by Ub-based DUB ABPs. Immunoblotting was performed using indicated antibodies, and GAPDH was used as a loading control.

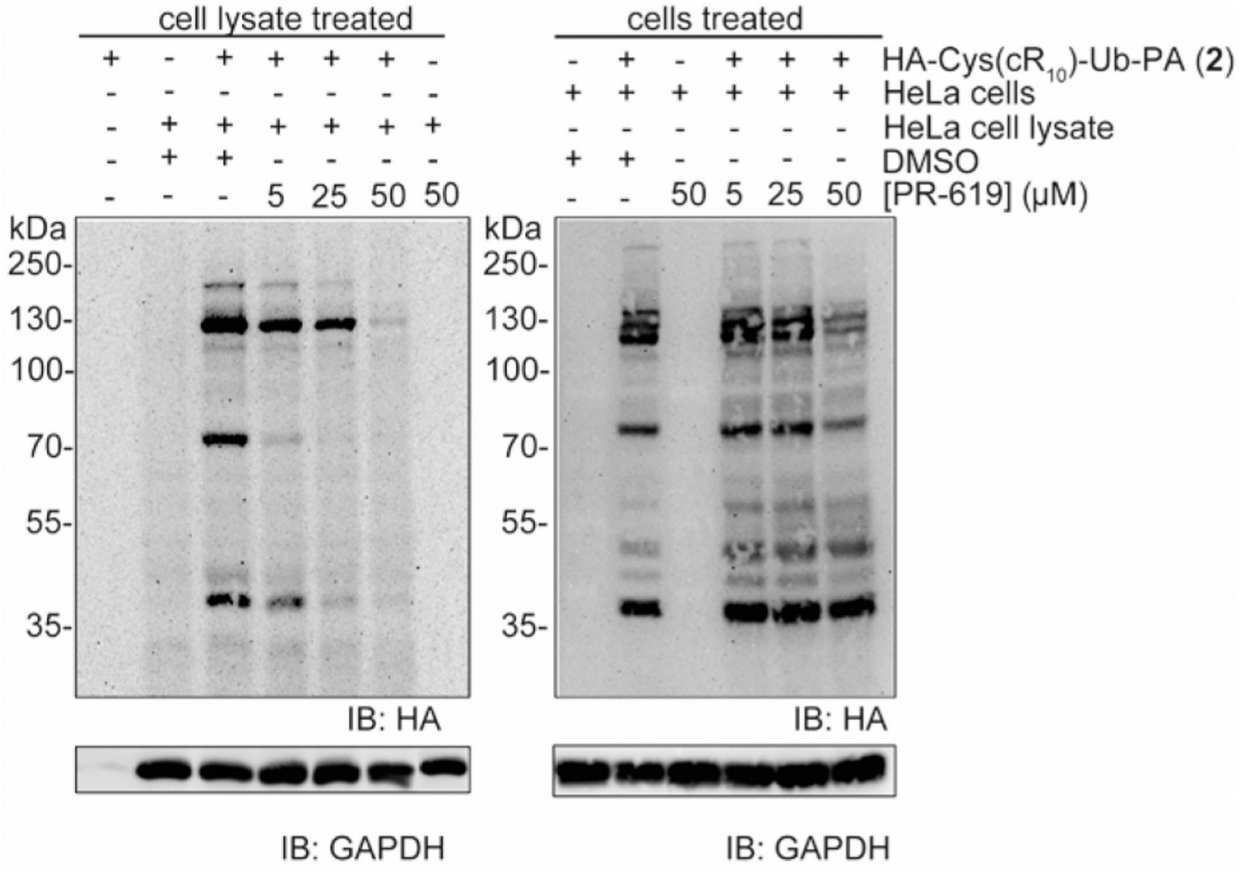

Figure 6.

Inhibition of intracellular and cell lysate DUB profiling by 15 μM HA-Cys(cR$_{10}$)-Ub-PA (**2**) using PR-619. Labeled DUBs were detected using anti-HA antibody. GAPDH was utilized as a loading control detected with anti-GAPDH antibody.

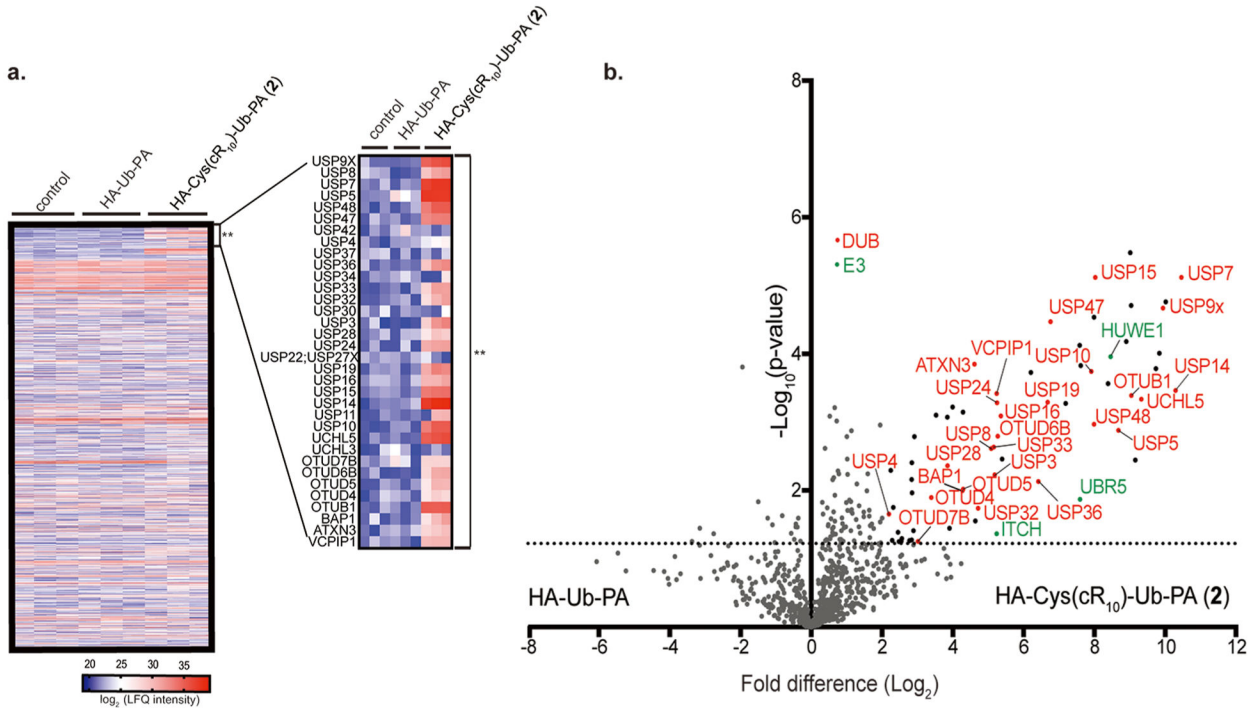

Figure 7.

Identification of pulled-down DUBs from HeLa cells treated with 15 μM HA-Cys(cR$_{10}$)-Ub-PA (**2**) for 4 h analyzed using MS-based LFQ. (a) Heat map representing the LFQ intensity scores of 1114 identified protein groups from samples corresponding to the control, cellular treatment of 15 μM HA-Ub-PA, or cellular treatment of 15 μM HA-Cys(cR$_{10}$)-Ub-PA (**2**). Each subcolumn contains repeats for each of the pulldown. Asterisks (**) denote the region corresponding to the DUBs. Inset shows a zoomed-in view of the DUBs within the heat map. Red represents enrichment (higher LFQ intensity (log$_2$)), where lack of enrichment (lower LFQ intensity (log$_2$)) is shown in blue. (b) Volcano plot of pairwise comparison of protein groups pulled down with HA-Cys (cR$_{10}$)-Ub-PA (**2**) relative to HA-Ub-PA.